Spatially disaggregated model for self-channel interference in mixed fiber optical network segments

Spatially Disaggregated Model for Self Channel Interference in Mixed Fibers Optical Networks Segments

EMANUELE VIRGILLITO[1,*], ANDREA CASTOLDI[2], ANDREA D'AMICO[1], STEFANO STRAULLU[3], ANDREA BOVIO[2], ROSANNA PASTORELLI[2], AND VITTORIO CURRI[1]

[1] Politecnico di Torino, Corso Duca degli Abruzzi, 24, Torino, Italy
[2] SM-Optics, U Via John Fitzgerald Kennedy, 2, Vimercate, Italy
[3] LINKS Foundation, Via Pier Carlo Boggio, 61, Torino, Italy
[*] Corresponding author: emanuele.virgillito@polito.it

Compiled May 25, 2023

Coherent transmission technology is widely diffused in backbone optical uncompensated transmission (UT) networks segments. In the metro and access network segments instead intensity-modulated direct detected channels at 10 Gbps requiring inline dispersion compensation units (DCU) are still largely used. While the transition to coherent technology is foreseen in the dispersion managed (DM) network segment, in the meantime it would be handy to route coherent channels through dispersion managed network segments to fully exploit deployed hardware and available spectrum and improve network flexibility. In this scenario, the self channel interference (SCI) exhibits a strongly coherent accumulation due to the presence of DCUs, which is not well modeled by traditional analytical models for non-linear interference estimation used for path feasibility assessment. In this paper we propose a semi-analytical model able to fill this gap. We show that our proposed model is able to provide a quick, conservative estimation of the SCI noise on both UT and DM systems, including OLS configurations with mixed fiber types.

http://dx.doi.org/10.1364/ao.XX.XXXXXX

1. INTRODUCTION

Dual Polarization coherent transceiver based on digital signal processing (DSP) have been widely deployed in the last years and dominate the backbone network segment on optical line systems (OLS) made up of uncompensated transmission (UT) fiber spans. State of the art coherent transceivers deliver up to 800 Gbps and recent technology advancements enabled up to 400 Gbps on CFP-2 pluggables using 64 GBaud on the 75 GHz DWDM grid modulated with DP-16QAM for the short reach and long haul accordingly to the OpenZR+ standard [1]. Meanwhile, the access and metro network segments, covering areas of tenth to hundreds of kilometers, are still largely served by legacy intensity modulated direct detected (IMDD) transceivers transmitting at 10 Gbps on dispersion managed (DM) OLSs with dispersion compensating units (DCU). The introduction of flexible rate coherent DSP receivers able to digitally compensate chromatic dispersion, track the channel transmission matrix changes and linearly map the BER performance to the optical signal-to-noise ratio (SNR) enabled the possibility for dynamic, autonomous optical network reconfiguration [2–4]. Indeed, in legacy IMDD systems the OLS configuration was static and tightly coupled to the spectral load, with an optical dispersion compensation scheme set to optimize its transmission. In modern coherent systems instead, the OLSs are becoming a shared commodity providing optical transport functionality [5]. This possibility has pushed optical networks towards openness [6–8] and disaggregation [9, 10], with the aim of providing features as network slicing, virtualization [11] and dynamic reconfiguration [4]. To fulfill traffic request, modern coherent transceivers are able to adapt their symbol rate and modulation format accordingly to the available quality of transmission (QoT).

While the upgrade of metro and access network segments to coherent technologies is certainly foreseen, network operators pursue the return of investment maximization of the deployed hardware and fiber. In this scenario, the possibility to route coherent lightpaths (LP) through DM network segments already carrying legacy IMDD traffic would certainly represent a good opportunity to improve network flexibility and save on capital expenditures. This scenario is depicted in Fig.1: the candidate path feasibility evaluation requires the computation of a QoT figure - the generalized SNR (GSNR) - by means of a quality of transmission estimator (QoT-E) [12]. In the optical network controller, the physical layer topology is abstracted using a graph whose nodes are the channels' add-drop sites, while the edges are the OLSs weighted by their GSNR degradation. The QoT-E interacts with the OLS controller to gather information about

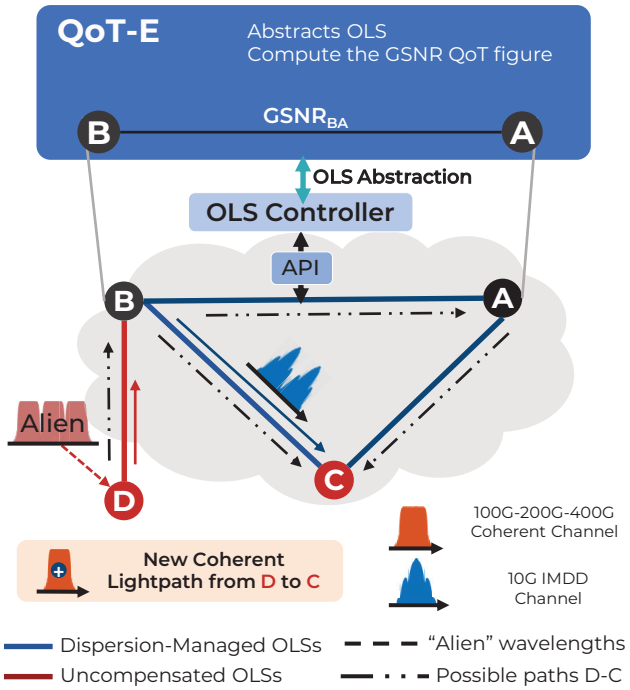

Fig. 1. Use case of LP deployment from node D to C. The physical layer is composed of UT (red) and DM (blue) OLS. DM OLSs may be already loaded with legacy 10G traffic. UT segments may carry also alien wavelengths whose full characterization may be not known.

OLS using open application programming interfaces (API) and estimates the available QoT. This requires a (semi-)analytical modeling tool able to evaluate all the possible source of impairment which may degrade the GSNR almost in real-time. Among of these, one of the main impairment is the non-linear interference (NLI) due to Kerr effect, which has been shown to be well modeled as an additive noise source for coherent LPs in UT systems [13, 14]. The NLI noise is made up of the self-channel interference (SCI) and cross-channel interference (XCI), respectively produced by a channel under test (CuT) on itself and by the other co-propagating channel on the CuT [13, 15, 16]. The broad family of the frequency domain gaussian noise (GN) model [14, 17–20] has been shown effective in predicting the NLI noise intensity in UT systems. Other approaches based on time domain have been proven to deliver equally good estimations [15, 21, 22]. In particular, the incoherent gaussian noise (IGN) model possess some features which makes it very attractive to be used for real-time QoT estimation as a path feasibility assessment tool. Indeed, it provides quick, conservative and spatially disaggregated NLI estimations, independent on the propagation history and allows spectral separation of XCI and SCI effects on a given CuT [16, 23]. Moreover, it has been implemented in available open source QoT-E tools, such as GNPy [24, 25], which has been widely tested in green- and brown-field optical system with UT fiber spans [4, 12, 26, 27]. The spectral and spatial separation features are crucial in open and reconfigurable networking since in practical scenarios not all the channel characteristics or their propagation history are known. Moreover, especially in the metro segment, OLS are likely far from being uniform, whilst being composed of mixed fiber types.

This work is focused on the SCI accumulation of a coherent LP in a generic OLS which may have both DM and UT segments. The XCI noise due to other co-propagating coherent channels in DM OLSs requires an in-depth study out of the scope of this article. The XCI effect caused by IMDD 10 Gbps channels on a coherent LP arising in joint propagation on a DM OLS has been already investigated and modeled in [28]. Indeed, the SCI has been shown to exhibit coherent accumulation in UT systems [13, 15], where is yet limited thanks to the large amount of accumulated dispersion at each span. However, a proper estimation of the SCI coherence in UT systems is still important due to the market trend to the symbol rate enlargement, which may make SCI comparable to XCI in some cases. Instead, when considering a DM OLS, due to the presence of DCU which limit the amount of chromatic dispersion accumulated in each span [13, 17], the coherent SCI accumulation becomes far stronger. In this scenario, the GN model hypotheses may not hold anymore, as the take on to a gaussian distributed signal (the signal *gaussianization*) is far slower. Actually, the coherent accumulation is to a certain extent considered in the coherent GN (CGN) [13] model version as well as in the time domain approach of [15], however, they do not provide a spatially separated approach supporting mixed fibers OLS. A correction for signal non-gaussianity, including also the coherent accumulation has been proposed in the enhanced GN model (EGN) [29, 30], but it is still based on a spatially aggregated approach and it has a large computational complexity. In this paper, extending the work presented in [31], we propose a semi-analytical model, based and validated upon an extensive numerical simulation campaign based on the split-step Fourier method (SSFM), aimed at the SCI coherent accumulation assessment, tailored for network operations in both DM and UT OLSs made up of mixed fiber types. In section 2 we briefly introduce the QoT estimation background and the requirements in terms of spectral and spatial disaggregation that a QoT-E tool for path feasibility should satisfy for efficient network operation. In section 3 we describe the general OLS configuration and its system abstraction on the base of which we have developed our model. We also describe the method to extract from SSFM simulations the significant metrics for the SCI accumulation. We show that SCI cannot be generally approached as a spatial disaggregated phenomenon due to its coherent accumulation, especially in DM OLS. Then, in section 4 we present the developed analytical approach for coherent SCI accumulation estimation, based on the statistical correlation of the intrinsic SCI noise fields introduced by each OLS span. In section 5 we first present the simulation method that we have developed to observe separately the SCI coherency features. We then present the results of an extensive simulation campaign, testing several uniform and mixed fiber types OLS configuration, together with different symbol rates and modulation formats, validating the approach presented in section 4. Section 6 illustrates that the model's correlation coefficients describing the amount of coherent SCI accumulation can be quickly estimated in a semi-analytical manner by knowing the CuT and OLS physical parameters. We also provide a further model test on a non-transparent, mixed fiber OLS configuration. As a further operative verification, in section 7 we show how neglecting SCI coherency may impact the final GSNR estimation and demonstrate that the proposed model can successfully correct the prediction. Finally, in section 8 we draw our conclusions.

2. SPECTRALLY AND SPATIALLY DISAGGREGATED QOT ESTIMATION

In this section we briefly focus on the disaggregation proper-

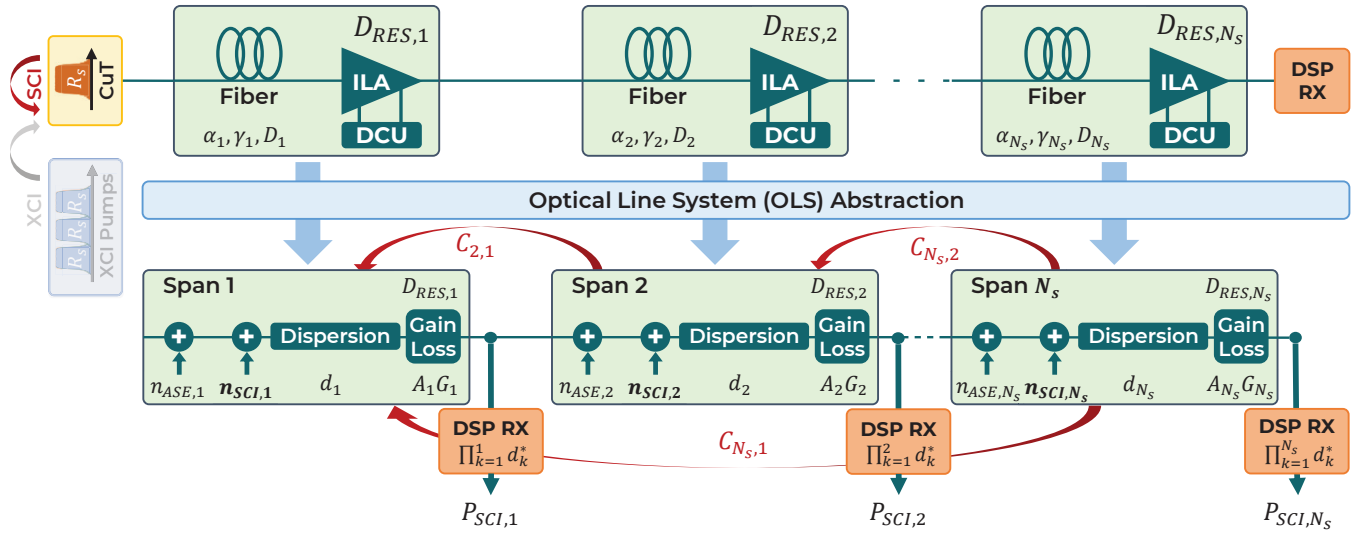

Fig. 2. Schematic of the considered generic N_s span OLS (upper). Each span may have different physical parameters. In the bottom part, the system block diagram abstraction used for GSNR calculation and SSFM observation.

ties of a QoT-E to be used in the context of modern network management and orchestration. A foreseeable use-case is represented in Fig.1. For the sake of simplicity we have represented a simple triangular meshed topology as an example of typical terrestrial meshed networks. As common in the metro and regional segments, the network is made of sections of modern UT OLSs tailored to coherent transmission as well as by DM OLS to support transmission of legacy 10G IMDD channels, which require DCUs placed at about each span. In the UT segment we may have some alien wavelength propagated on a portion of the spectrum leased to a certain operator. In this case, the characteristics of such signals, such as their modulation format, may be unknown. In the DM segments instead we may have a spectrum section already populated with legacy 10G traffic. In this context, we consider the deployment of a coherent LP from node D to C, thus needing to be routed through a path made up, in general, of both DM and UT OLSs. The QoT-E relies on a (semi-)analytical model to check the candidate paths feasibility with respect to a certain requested bit-rate and to set the transceiver operational mode (modulation format and symbol rate). It has been shown that for coherent channels the GSNR can be used as the QoT figure [12], as it can be mapped back to the pre-FEC BER using the transceiver BER vs GSNR performance curves [25]. The GSNR takes into account both the amplified spontaneous emission (ASE) noise P_{ASE} introduced by inline amplifiers (ILA) and the NLI power P_{NLI} due to Kerr effects for a CuT with power P_{ch} :

$$GSNR = \frac{P_{ch}}{P_{ASE} + P_{NLI}} = \left(\frac{1}{OSNR} + \frac{1}{SNR_{NLI}}\right)^{-1} \quad \textbf{(1)}$$

$$OSNR = \frac{P_{ch}}{P_{ASE}} \qquad SNR_{NLI} = \frac{P_{ch}}{P_{NLI}}$$

where the $OSNR$ due to the ASE noise and the SNR_{NLI} due to NLI can be considered separately. As mentioned in section 1, in UT systems, the NLI noise is composed of the SCI and XCI. XCI is generated by each single pump channel on the CuT [13, 16], and the contributions of each channel can be summed in power. Four-Wave Mixing (FWM) instead is considered negligible as long as phase matching does not occurs as in fibers with large to moderate dispersion coefficients [16, 21, 23]. This feature allows the NLI to be treated as a spectrally disaggregated effect, so that each interfering channel maps to an additional QoT degradation on the CuT, independently on the other channels. This is a huge simplification of the QoT estimation, allowing to logically separate portion of the spectrum. Hence, the SNR_{NLI} for N_p interfering XCI pumps can be written as:

$$\frac{1}{SNR_{NLI}} = \frac{1}{SNR_{SCI}} + \sum_{k=1}^{N_p} \frac{1}{SNR_{XCI,k}} \quad \textbf{(2)}$$

Moreover, in UT systems both SCI and XCI can be substantially modeled as spatially disaggregated phenomena. This means that the amount NLI introduced by each span rapidly converges to an asymptotic value which is independent on the previous propagation history of both the CuT and the interfering channels [16]. This is another important feature for real-time usage of QoT-E tools, as the propagation history of alien wavelengths may be not known and it further allows easy QoT estimation in realistic scenarios where the OLSs may be composed of fiber spans of different type and length. Hence, spectral/spatial disaggregation are key features of NLI generation in UT systems as well as the capability of GN model to provide a conservative estimation ensuring to operate on the safe side [25]. However, when dealing with DM OLS, the GN model approach is known to not hold anymore due to the small amount of net dispersion accumulated over the OLS [17]. Hence, we should first observe the NLI generation in the DM regime to test whether the spatially and spectrally disaggregation features hold.

3. OPTICAL LINE SYSTEM ABSTRACTION

To assess the spectral and spatial disaggregation properties of NLI accumulation we have carried out a preliminary set of SSFM simulations. We first describe the generic OLS configuration and the employed method to observe the NLI buildup along the OLS. The generic OLS, represented in Fig.2, is made up of N_s fiber spans. Each fiber span is a sequence of an optical fiber, DCU and ILA. We target a realistic scenario made up of different

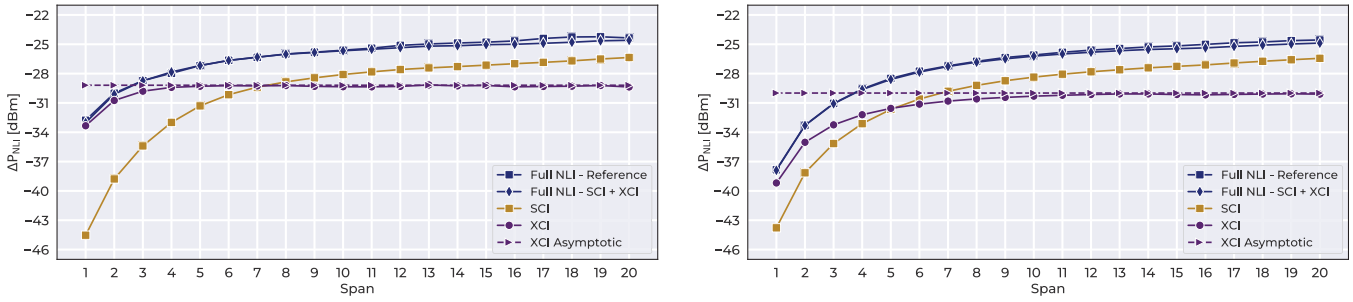

(a) $D = 4$ ps/nm/km - $D_{RES} = 90$ ps/nm

(b) $D = 16$ ps/nm/km - $D_{RES} = 90$ ps/nm

Fig. 3. Amount of NLI components introduced by each span on the CuT for a 20x span uniform OLS with $D_{RES} = 90$ ps/nm and (a) $D = 4$ ps/nm/km (b) $D = 16$ ps/nm/km. Other physical parameters are identical: $L_s = 80$ km, $\alpha = 0.2$ dB/km, $\gamma = 1.27$ 1/W/km. Asymptotic XCI value is calculated as the average of the ΔP_{XCI} from 10th to 20-th span.

fiber types and non-transparent amplification, the The i-th fiber span has loss coefficient α_i [dB/km], dispersion coefficient D_i [ps/nm/km] (or equivalently expressed in terms of frequency as $\beta_{2,i}$ [ps/THz/km]), non-linear coefficient γ_i [1/W/km] and length $L_{s,i}$ [km], being $i = (1 \dots N_s)$. The DCU defines the dispersion compensation scheme of a DM OLS introducing a certain amount of negative accumulated chromatic dispersion $D_{DCU,i}$ [ps/nm] (or, $\beta_{DCU,i}$ [ps/THz]) which summed to the fiber accumulated dispersion $D_i \cdot L_{s,i}$ sets the in-line residual dispersion $D_{RES,i}$ left at the end of the i-th span:

$$D_{RES,i} = D_i \cdot L_{s,i} + D_{DCU,i} \tag{3}$$

Hence, such definition is generic as when $D_{DCU,i} = 0$ ps/nm we describe an UT fiber span with $D_{RES,i} = D_i \cdot L_{s,i}$ ps/nm. We consider the non-linearity introduced by the DCU negligible, as these are usually inserted between two amplifier stages and its input power is set as low to operate in linear regime. Each fiber span thus accumulates a span loss $A_i = \alpha_i \cdot L_{s,i}$ dB which is recovered by the ILA gain G_i. When the OLS is operated in transparency $A_i G_i = 1$ (in linear units), however, in realistic OLSs, it is common to not have this condition met. To isolate the NLI/XCI/SCI noise power, we assume ideal amplification by turning off the ASE noise generation in simulations. We then place a coherent DSP receiver at the end of each fiber span to observe the evolution of the noise power. The coherent DSP receiver first performs chromatic dispersion compensation (CDC), which is done ideally as in simulations we know exactly how much dispersion has been accumulated up to the i-th span. The CDC stage is followed by a least mean square (LMS) adaptive equalizer with 42 taps and an adaption coefficient $\mu = 10^{-4}$, followed by an carrier phase estimation stage completely recovering the non-linear phase noise. Although such large number of equalizer taps is unrealistic, they ensure a large back-to-back simulation SNR allowing observation of small noise powers. The SNR in the symbol rate bandwidth R_s is finally estimated on the constellations at 1 sample per symbol at the CPE output.

On the optical signal side, we will consider here square-root raised cosine shaped signals with 15% roll-off, modulated at $R_s = 32$ Gbaud and 64 Gbaud, using DP-QPSK and DP-16QAM modulation format at $P_{ch} = 1$ dBm, thus covering deliverable rates of 100Gbps, 200Gbps and 400Gbps as in commercially available flexible-rate transceivers. Hence, given the spectral and OLS configurations, we are able to gather the curves describing the accumulated $SNR_{NLI,i}$ up to the i-th span, from which we extract the accumulated NLI power $P_{NLI,i}$ by inverting the SNR_{NLI} definition. To study the spatial disaggregation property, however, it is necessary to evaluate the amount of NLI power introduced by the i-th span $\Delta P_{NLI,i}$, which is estimated differentially from the accumulated values:

$$\Delta P_{NLI,i} = P_{NLI,i} - P_{NLI,i-1} \tag{4}$$

Hence, whether the Eq.4 refers to overall NLI, SCI or XCI depends on the simulated spectral configuration, so that we can test the spectral/spatial disaggregation properties.

To check it on a DM OLS we have simulated the propagation on a uniform, transparent OLS of $N_s = 20$ spans with $D_{RES} = 90$ ps/nm obtained with two fiber dispersion coefficient valued D of 4 ps/nm/km and 16 ps/nm/km. The spectrum is loaded with $N_{ch} = 21$ 100G channels using DP-QPSK and $R_s = 64$ Gbaud, being the center channel (11th) the CuT. We have carried out three types of simulations: the *multichannel* case simulates the propagation of 21 channels at the same time with $P_{ch} = 1$ dBm launch power to observe the evolution of the whole NLI noise in DM OLS. We then simulate the *single channel* propagation of the CuT alone to isolate $\Delta P_{SCI,i}$. Then, we simulate the *pump and probe* scenario, with the CuT propagated at the same time with one of each XCI pumps, keeping the CuT power at $P_{ch} = -20$ dBm to isolate the XCI. We thus obtain the $\Delta P_{XCI,k,i}$ noise power curve of the k-th pump at the i-th span. The SCI and XCI noise powers obtained with single channels and pump and probe simulations are then summed using Eq.2 to reconstruct the overall NLI. As the SCI-XCI superposition is not the main target of this article, more information can be found on [16, 23]. In Fig.3 we report the amount of NLI, SCI, XCI (depending on the simulation type) introduced by each fiber span (i.e. the NLI gradients $P_{NLI,i}$, $\Delta P_{SCI,i}$, $\Delta P_{XCI,i}$). The comparison of the NLI gradient $\Delta P_{NLI,i}$ obtained by multichannel simulation with the superposition of the SCI and XCI (blue curves) shows that the overall NLI is composed by these two phenomena even in DM OLS so that Eq.2 holds as spectral disaggregation. We can also note that the XCI noise converges to an asymptotic, worst-case value after a transient of some spans, thus confirming also spatial disaggregation for XCI effect. With respect to SCI noise power instead we observe that its amount per span continuously grows with no asymptotic value, confirming that SCI in DM OLS is not, in general, a spatially disaggregated phenomenon, which instead requires the knowledge of the CuT propagation history to be properly estimated. Indeed, as already mentioned, the

coherent accumulation of SCI is a well known fact [13, 17, 19, 32, 33] which has been treated mainly for uniform OLSs. However, in the next section we will propose a novel semi-analytical model supported by extensive SSFM-based observation, tailored to the estimation of the SCI in OLSs made up of mixed fiber types and including both DM and UT schemes.

4. SCI DISAGGREGATED MODELING

In the previous section we have shown the the amount of $\Delta P_{SCI,i}$ introduced by each span keeps increasing even in a uniform OLS where all the fibers are equal, thus suggesting that it is a spectrally aggregated phenomenon. Indeed, even if to a lower degree, this has been shown in [34] even in UT systems. However, for network online management it would be handy to have a spatially disaggregated approach, similarly to that of the IGN model, giving the amount of SCI per span. However, it is clear that this approach cannot work in DM OLS. The theory of the CGN model [13, 17] gives us some insights on this, suggesting that such increase of power is due to a coherent accumulation of the SCI noise contributions from different spans caused by the accumulated phase shifts deriving from previous spans' accumulated dispersion. Intuitively, the large coherency between different SCI spans contributions in DM OLSs is caused by the small net amount of accumulated dispersion due to DCU compensation at each span, which avoids rapid pulse spreading. Hence, since SCI is actually related to the signal time evolution, the contributions from different spans sum up coherently to a degree which depends on the accumulated dispersion. On the other side however, the CGN model and its evolution such as the EGN model [29, 30], must keep an aggregated approach as the phenomenon itself is. However, they are mostly tailored to work with uniform OLSs, rarely found in practical terrestrial networks, and they may have higher computational complexity. Note that whatever the model, taking into account coherent accumulation would in any case complicate the QoT estimation. However, while for XCI this would have been a crucial point as it is not possible, in general, to know the propagation history of all the DWDM channels, it can be instead tolerated for SCI, especially in the path computation phase, because the configuration of the candidate path itself is known. We thus need to find a sufficiently accurate, conservative approach allowing to calculate separately the coherency contribution in mixed fiber OLSs, yet retaining a reasonable complexity and small execution time. Here, we propose to approach the coherency problem as the estimation of the correlation between the SCI stochastic noise processes introduced by span, i.e. the *pure* SCI components, intrinsic to each span and solely on them, rather than considering the overall accumulated SCI process which implies a spatially aggregated approach. Indeed, although the Kerr effect is a distributed phenomenon arising along fiber propagation, at least for fibers exceeding the effective length, the whole GN model family theory model the SCI as an equivalent additive, gaussian noise source at the fiber span input. Hence, the main idea is to split the SCI estimation problem in two: first, the pure SCI intensity estimation; second, the evaluation of the additional power due to their coherent interaction, whose degree depends on the dynamics of the dispersion accumulated between the two pure SCI processes summing up coherently at the receiver.

To develop an SCI model based on this idea we thus need a linearized system block diagram of the OLS taking into account the dispersion contributions, as reported in the bottom part of Fig.2. Here, $n_{SCI,i}(t)$ is the i-th span pure SCI noise field stochastic process introduced at the end of the span and equivalently moved to the fiber input. Considering the SCI noise field of the i-th span, its power ${\sigma_{SCI,i}}^2$ is the expectation $E[\cdot]$ of its square modulus:

$$ {\sigma_{SCI,i}}^2 = E[|n_{SCI,i}(t)|^2] \tag{5} $$

From now on, we will omit the SCI subscript and the time dependency for notation's clarity and conciseness. The final SCI impact on the GSNR is due to the sum of noise contributions introduced by all the spans. However, while in XCI the span contributions can be considered completely uncorrelated among themselves, this is not true for the single channel effect, so that the correlation component is non-negligible.

To consider this effect, in each span block we add a multiplicative, complex coefficient d_i accounting for the accumulated phase due to the i-th span chromatic dispersion, including DCU if any, which has the property $|d_i|^2 = d_i \cdot d_i^* = 1$. Hence, each pure SCI noise field is multiplied by those coefficients, as well as by the gain-loss product $A_i G_i$, which is not unitary in the most general case of non-transparent OLS. Each span noise field contribution n_i thus undergoes this dispersion and gain-loss terms and all of the subsequent spans as it propagates throughout the OLS. At the receiver, placed at the end of the i-th span, the CDC stage ideally applies a phase filter whose transfer function is the complex conjugate of the dispersion accumulated up to that span, i.e. $\prod_{n=1}^{i} d_n^*$ Hence, the accumulated SCI noise field at the i-th span receiver, after CDC, is:

$$ \bar{n}_i(t) = \sum_{k=1}^{i} \left(n_k(t) \cdot \prod_{j=k}^{i} \sqrt{A_j G_j} \cdot \prod_{n=1}^{k-1} d_n^* \right) \tag{6} $$

For example, at the end of the first three spans we have:

$$ \begin{aligned} \bar{n}_1 &= \sqrt{A_1 G_1}\, n_1 \\ \bar{n}_2 &= \sqrt{A_2 G_2} \left(\sqrt{A_1 G_1}\, n_1 + d_1^* n_2 \right) \\ \bar{n}_3 &= \sqrt{A_3 G_3} \left(\sqrt{A_2 G_2\, A_1 G_1}\, n_1 + \sqrt{A_2 G_2}\, d_1^* n_2 + d_1^* d_2^* n_3 \right) \end{aligned} \tag{7} $$

Then the total SCI power at the end of the i-th span $P_{SCI,i}$ is obtained as the expectation of the square modulus of the accumulated SCI field $\bar{n}_i$.

$$ P_{SCI,i}(t) = E[|\bar{n}_i(t)|^2] \tag{8} $$

By developing the calculus it can be demonstrated that the accumulated $P_{SCI,i}$ can be generally written as:

$$ P_{SCI,i} = A_i G_i \left(P_{SCI,i-1} + \Delta P_{SCI,i} \right) \tag{9} $$

$$ \Delta P_{SCI,i} = {\sigma_i}^2 + 2 \sum_{j=1}^{i-1} {\sigma_{ij}}^2 \prod_{k=j}^{i-1} \sqrt{A_k G_k} \tag{10} $$

$$ {\sigma_{ij}}^2 = E\left[\mathfrak{Re}\left(n_i\, {n_j}^* \prod_{k=j}^{i-1} d_k^* \right) \right] \tag{11} $$

Eq. (9) expresses conveniently the accumulated SCI power as the sum of the previous span power and the amount of additional power $\Delta P_{SCI,i}$ of the i-th span, which includes coherency. As $\Delta P_{SCI,i}$ is multiplied by $A_i G_i$, it thus represents the additional i-th span SCI power as if it was placed at the fiber input, so that is the quantity we want to model and compare to the SCI curve of 3. From Eq. (10) and Eq. (11), $\Delta P_{SCI,i}$ is made up of two terms. The first term ${\sigma_i}^2$ is the *pure* SCI power, i.e. the power of the

process generated at the i-th span (Eq. (5)). The second term instead describes the coherency arising from the double products of the square modulus in Eq. (8). Let us define the i-th span as the *Span under Test* (SuT), i.e. the span we calculate the total introduced SCI power for. The second term in Eq. (10) sums up the correlation of the SuT (i-th) pure SCI with all the j-th preceding spans ($j = 1 \dots i-1$), each of them indicated as *Correlated Span* (CrS). This approach separates the terms contributing to the total SCI power on a per span basis, adding the correlation of the SuT with each of the preceding CrS on top of the SuT pure SCI, where the latter can be estimated independently on the other OLS spans. The correlation between the SuT and CrS spans (i, j) is the ${\sigma_{ij}}^2$ term of Eq. (11), where $\mathfrak{Re}$ stands for the real part operator of a complex quantity. Eq. (11) shows that this quantity depends on the amount of net chromatic dispersion accumulated from the CrS (j-th span) up the beginning of the SuT (i.e. up to the span $i-1$). Note that the dispersion count includes the DCUs, hence it is determined by the sum of the span inline residuals $D_{RES,k}$, $k = (j \dots i-1)$ in DM OLSs, while it matches the fiber accumulated dispersion in UT OLSs.

Although an analytical approach to the ${\sigma_{ij}}^2$ estimation may be possible, it will investigated in future works. Here instead we approximate the Eq. (11) by rewriting with respect to the the correlation coefficient in order to express it as a function of the pure SCI powers:

$$ {\sigma_{ij}}^2 \approx C_{ij}\, \sigma_i\, \sigma_j \tag{12} $$

With this approximation, the general $\Delta P_{SCI,i}$ formula at the dn of the first three span, for a generic, non-transparent OLS gives:

$$ \begin{aligned} \Delta P_{SCI,1} &= {\sigma_1}^2 \\ \Delta P_{SCI,2} &= {\sigma_2}^2 + 2\sqrt{A_1 G_1}\, C_{21}\, \sigma_2\, \sigma_1 \\ \Delta P_{SCI,3} &= {\sigma_3}^2 + 2\sqrt{A_2 G_2\, A_1 G_1}\, C_{31}\, \sigma_3\, \sigma_1 + 2\sqrt{A_1 G_1}\, C_{32}\, \sigma_3\, \sigma_2 \end{aligned} $$

Moreover, in a transparent ($A_i G_i = 1$), uniform OLS, as it will be discussed in the next section, the formula simplifies as:

$$ P_{SCI,i} = \left(P_{SCI,i-1} + \Delta P_{SCI,i}\right) \tag{13} $$

$$ \Delta P_{SCI,i} = {\sigma_i}^2 + 2 \sum_{j=1}^{i-1} C_{ij}\, \sigma_i\, \sigma_j \tag{14} $$

In Eq. (12) we assume that the amount of additional coherency power may be expressed as the product of the standard deviations of the pure SCI terms, scaled by a correlation coefficient C_{ij} such that $0 < C_{ij} < 1$, whose value should scale down mainly with increasing accumulated dispersion between j-th and i-th span. This implies that, as long as D_{RES} in not zero, the C_{ij} should decrease as farther are the spans (i, j) one from each other. Hence, when the C_{ij} are nearly zero, as in UT systems with high dispersion fiber, coherence tends to zero and SCI can be modeled as a spatially disaggregated phenomenon using only the pure terms σ_i , independent on propagation history. When C_{ij} terms are not negligible instead, as in DM OLSs, the propagation history may not be neglected. However, as the C_{ij} are assumed to scale with accumulated dispersion, their value should decrease rapidly as we consider the correlation of farther span, so that the coherence may exhaust after a certain spatial memory.

It should be noted that the case of Raman amplification may pose some non trivial complications in the mechanism of NLI and coherence generation, especially with counter-propagating Raman pumps which raises the signal power near the end of the fiber. If the Raman gain is large enough, it may trigger the generation of a significant additional amount of SCI near the end of the span, which may interact with the previous contribution in a more complex manner due to the additional dispersion accumulated within the fiber span. Although operating Raman amplifiers is such high gain regime is not common, we consider the application of the model in this scenario as out of the scope of this paper and it will be object of future studies.

5. MODEL VALIDATION BY SSFM SIMULATIONS

Table 1. Uniform Configuration

CuT Configuration		
R_s	32, 64	GBaud
Predistortion	0, 102400	ps/nm
Uniform OLS Configuration - 20x Span		
α	0.15, 0.2, 0.25	dB/km
D	4, 16	ps/nm/km
D_{RES}	40, 80, UT	ps/nm
L_s	80	km

Table 2. Mixed Fiber Configuration

CuT Configuration		
R_s	32, 64	GBaud
Predistortion	0, 102400	ps/nm

Fiber Types	Length km	α dB/km	D ps/nm/km	γ 1/W/km
SSMF	80	0.15	16	1.27
NZDSF-1	80	0.20	8	1.46
NZDSF-2	80	0.25	4	1.92

Mixed Fiber OLS Configuration - 16x Span				
Module #	1	2	3	4
Module Name	**NZDSF-1**	**NZDSF-2**	**SSMF**	**MIXED**
Span 1	NZDSF-1	NZDSF-2	SSMF	SSMF
Span 2	NZDSF-1	NZDSF-2	SSMF	NZDSF-2
Span 3	NZDSF-1	NZDSF-2	SSMF	SSMF
Span 4	NZDSF-1	NZDSF-2	SSMF	NZDSF-2
D_{RES} per Fiber Module [ps/nm]				
Case #1	40	40	40	40
Case #2	UT	UT	UT	UT
Case #3	80	40	UT	40

The model presented in the previous section provides a spatially disaggregated approach to estimate the different contributions determining the overall coherent SCI power. In order to validate the model we have set up a validation methodology based on SSFM simulations able to extract both the C_{ij} and the

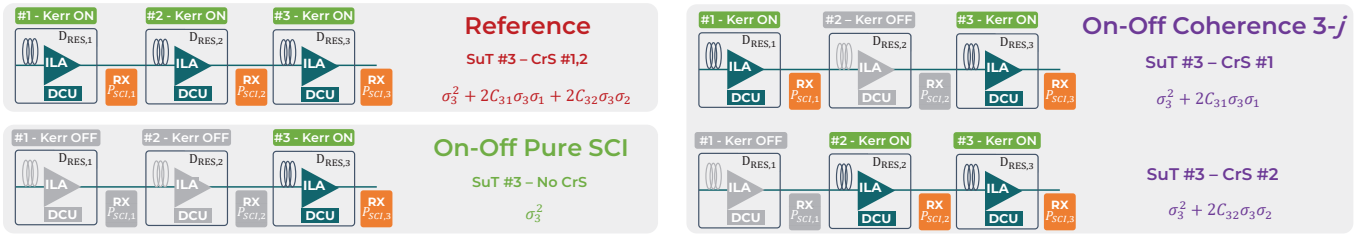

Fig. 4. Schematic of the three type of simulation carried out to isolate SCI components for a sample $N_s = 3$ span OLS.

pure ${\sigma_i}^2$ terms and reconstruct the overall ΔP_{SCI} introduced by each span using Eq. (10). Furthermore, the presented approach accounts also for OLSs with mixed fiber types. In this model validation phase we have considered several OLSs configuration, starting from the simplest case of uniform OLSs operated in transparency, to mixed fiber types OLS using fiber spans with different physical parameters and different inline residuals in the same OLS. Finally, we have tested the model also on an non-transparent OLS configuration mimicking an experimental setup in SM-Optics laboratories, although we have not been able to provide an experimental validation due to complications in amplifier setup with single channel loads. As far as uniform and transparent OLSs are concerned, all the gain-loss products A_iG_i are unitary and the model simplifies as in Eq. (14). In the uniform configurations, we have tested different residual values, both in the DM and UT regime, as well as different fiber dispersion coefficient and loss coefficient, although they remain constant in all the spans of each simulation run. The considered configurations are reported in Tab.1, together with the CuT configuration. Tab.2 reports instead the considered OLS configurations for the testing in a mixed fiber scenario. In this case, we have considered 3 types of fiber with different physical parameters. Although the loss coefficient is somewhat unrealistic, we opted to test fiber as much different as possible. The dispersion and non-linear coefficients represent those of common fibers as standard single mode fiber (SSMF) and non-zero dispersion shifted fiber (NZDSF) (Tab.2 Fiber Types). Note that fiber length has kept constant to $L_s = 80$ km because what matters in NLI generation is the accumulated dispersion and the effective length $L_{eff} = {1-e^{-\alpha L_s}}/{\alpha}$, whose effect can be observed with different D and α [13]. The mixed fiber OLS have been built as 4x modules of 4x span each, to a $N_s = 16$ total span count. The 1st 4x span module is always composed of all-equal NZDSF-1 fibers, the 2nd by NZDSF-2, the 3rd by SSMF and the 4th by alternated SSMF and NZDSF-2. With this fiber sequence we have then considered a completely UT system by removing all the DCUs (Tab.2, Case #2) and a completely DM system by setting DCU accordingly to the fiber type to obtain a constant D_{RES} = 40 ps/nm (Tab.2, Case #1), which is a typical value in legacy DM systems for IMDD. Finally, a mixed fiber types - mixed residual OLS (Tab.2, Case #3) has been considered by properly setting the DCUs in order to obtain different D_{RES} in each module but constant for all the 4x spans of each. The 1st, 2nd and 4th module have D_{RES} equal to 80, 40, and 40 ps/nm, respectively, the 3rd SSMF-like module is instead UT. The last scenario accounts for a coherent channel being routed through segments of UT and DM OLS with different fiber types to stress test the model performance.

A. SSFM Strategy

To validate the model for each configuration of CuT and OLS, we ran a simulation set composed by three types of simulations, outlined in Fig.4:. We have carried out a complete simulation set for all the combinations of parameters considered, although we will show only a subset of the results. In all the simulations we receive the channel at the end of all the fiber spans to extract the curve of the ΔP_{SCI} introduced by each span, as described in section 2.

- **Reference**: we propagate the CuT alone in the considered OLS with both chromatic dispersion and Kerr effect turned on in all the spans. This delivers the $\Delta P_{SCI,i}$ curve where each point counts the aggregated noise of pure SCI and its correlation with the previous span. It thus represent the reference curve of the whole effect.

- **On-Off - Pure SCI**: we propagate the CuT alone on the same OLS but turning off Kerr effect in all the span except the SuT (the i-th span), but leaving the accumulation of chromatic dispersion and DCUs. We thus obtain a set of N_s simulations, one for each SuT ($i = 1 \dots N_s$). Consequently, we observe only one SNR drop among all the span due to the i-th span generating SCI. Since all the other span have $\gamma = 0$ there is no coherent summing with other span contributions, but we retain solely the effect of previously accumulated dispersion on the intensity of the pure SCI term.

- **On-Off - Correlation Coefficients**: we propagate the CuT alone in the considered OLS but turning off Kerr effect in all the spans except the i-th and j-th, $j < i$. We do this for all the (i, j) span couples ($^{N_s(N_s-1)}/_2$ simulations per configuration). Consequently, at the i-th span we observe only the aggregated noise of the i-th and j-th pure SCI terms plus the additional power due to their correlation. Since we estimate the pure SCI terms from the previous simulations set, we can isolate the coherence power and thus estimate the C_{ij} as per Eq. (14).

From each set of simulations we can estimate all the ${\sigma_i}^2$ and C_{ij} and combine them together accordingly to Eq.10,11 to reconstruct the reference curve. A few comments must be done regarding the CuT configuration. Each simulation set has been done twice: once with the channel undistorted and then applying a predistortion of 102400 ps/nm. The *undistorted* case mimics the situation in which a channel is being deployed or regenerated at the beginning of the OLS. The *predistorted* case represents instead a channel which has accumulated some dispersion due to previous propagation. Such accumulated dispersion tends to *gaussianize* the signal [29] which generates more NLI, towards an asymptotic worst-case value which is well modeled by the

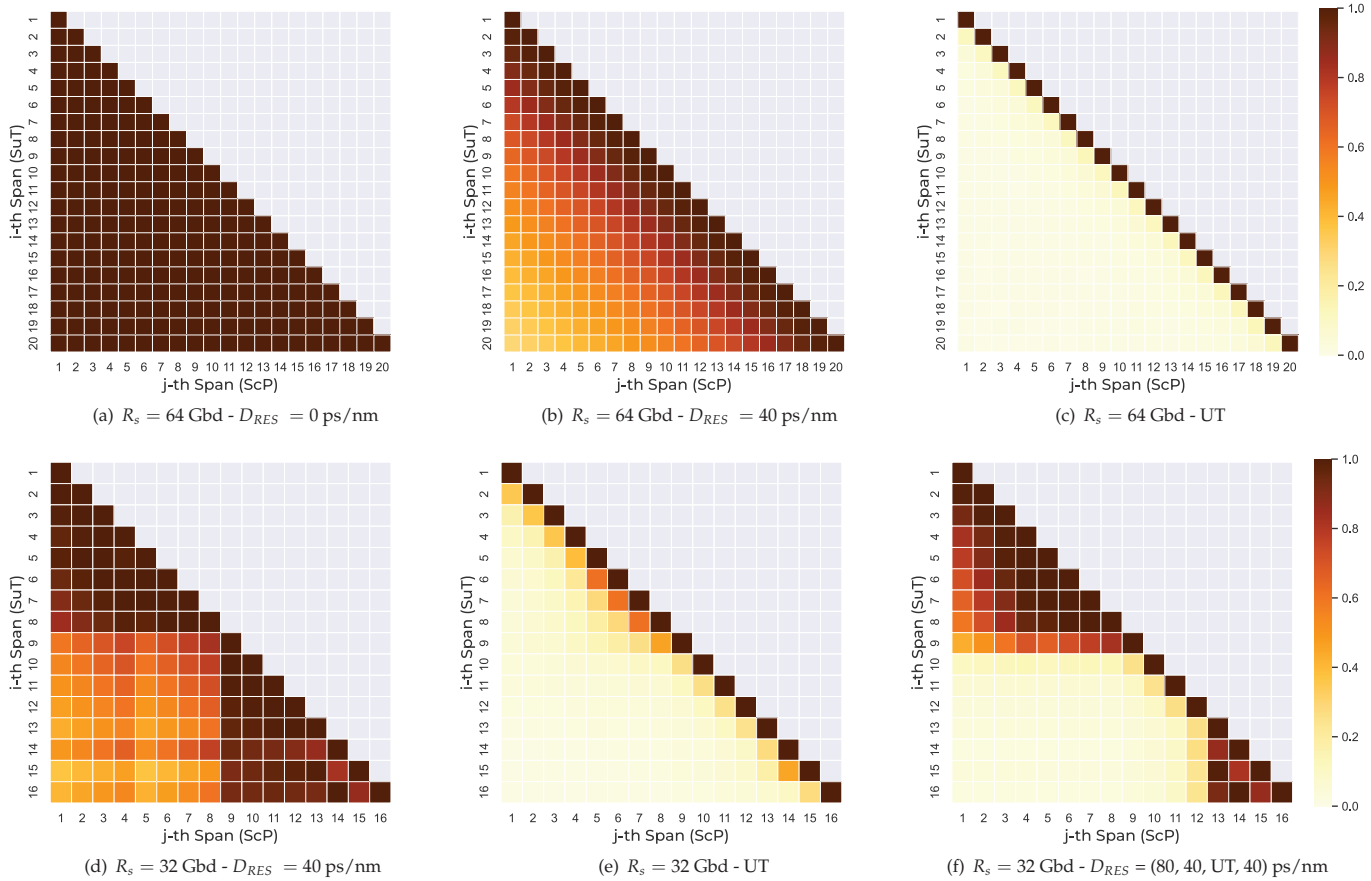

(a) $R_s = 64$ Gbd - $D_{RES} = 0$ ps/nm (b) $R_s = 64$ Gbd - $D_{RES} = 40$ ps/nm (c) $R_s = 64$ Gbd - UT

(d) $R_s = 32$ Gbd - $D_{RES} = 40$ ps/nm (e) $R_s = 32$ Gbd - UT (f) $R_s = 32$ Gbd - D_{RES} = (80, 40, UT, 40) ps/nm

Fig. 5. Representation of the correlation coefficients matrix $\bar{C}$ of the DP-QPSK, predistorted simulation set for a subset of configuration: (Upper row) Uniform OLS with $D = 4$ ps/nm/km and (Bottom row) mixed fiber OLS. Symbol rate and D_{RES} are reported in subcaption of each map.

IGN model, actually based on the signal gaussian distribution hypothesis. The convergence towards this value is known as *gaussianization*, which has already been studied and modeled by improved models of the GN family [35]. However, our simulation approach with the pure SCI curves allows also to isolate the gaussianization effect for SCI only, separately from coherency buildup.

B. Simulation Results

First, we can get a first glance at the coherence between each span couple (i, j) by building a **C** matrix whose rows represents the i-th span (the SuT) and the columns the i-th span (the CrS). Its elements are the correlation coefficient C_{ij} extracted from the on-off simulations set, with applied predistortion:

$$\mathbf{C} = \begin{bmatrix} C_{11} & 0 & 0 & \dots & 0 \\ C_{21} & C_{22} & 0 & \dots & 0 \\ C_{31} & C_{32} & C_{33} & \dots & 0 \\ \vdots & \vdots & \vdots & \ddots & \vdots \\ C_{N_s1} & C_{N_s2} & C_{N_s3} & \dots & C_{N_sN_s} \end{bmatrix} \quad \textbf{(15)}$$

where the elements on the main diagonal $C_{ii} = 1$ as they correspond to the pure SCI terms. The estimated **C** matrix has been represented as heatmap for a subset of example configurations on Fig.5. Darker color stands for larger C_{ij} value, hence stronger coherence. In the upper row three uniform OLS configurations with $R_s = 32$ GBaud, $D = 16$ ps/nm and $D_{RES} = 0$ ps/nm (Fig.5(a)), $D_{RES} = 40$ ps/nm (Fig.5(b)), UT (Fig.5(c)) have been reported. As expected, all the C_{ij} in the full compensation scenario ($D_{RES} = 0$ ps/nm) are unitary, meaning that the correlation is maximum for all the span couples as dispersion is fully compensated by DCUs at each fiber span. However, this is a purely theoretical case, strongly detrimental for system performance and that may also trigger a significant amount of FWM when considering multichannel propagation. Going to $D_{RES} = 40$ ps/nm and UT instead we see a decrease of correlation as the spans (i, j) are farther. However, while correlation is large up to nearly 10 spans of distance in the $D_{RES} = 40$ ps/nm case, correlation drops after a couple of spans in the UT case, confirming a small-to-negligible coherence in this case, with a spatial memory of around 1 span. The lower row instead reports the **C** matrix for the mixed fibers OLS with constant D_{RES} = 40 ps/nm (Fig.5(d)), UT (Fig.5(e)) and mixed residual (Fig.5(f)). Here we see how different fiber types, in particular w.r.t. to their dispersion coefficient D, impact the correlation entity. In the $D_{RES} = 40$ ps/nm case, we can notice that, although the residual is constant, the C_{ij} have some dependency on the dispersion coefficient: from Tab.2, the 9-th span is the first of the third mod-

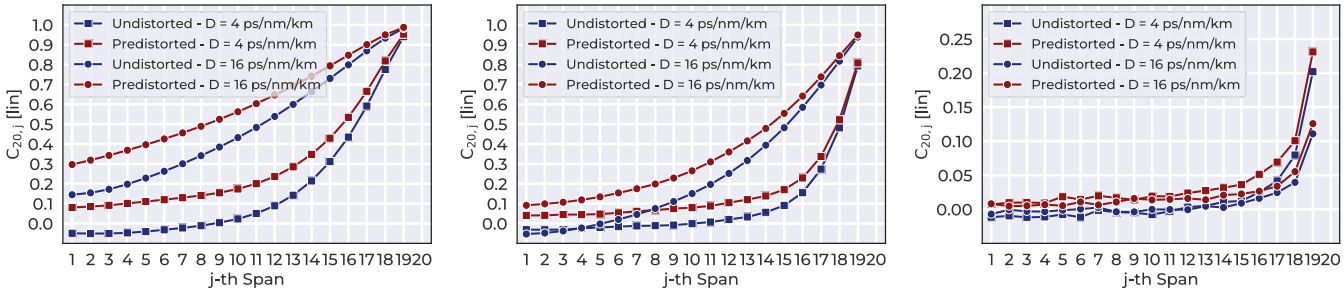

(a) $R_s = 64$ Gbd - $D_{RES} = 40$ ps/nm (b) $R_s = 64$ Gbd - $D_{RES} = 80$ ps/nm (c) $R_s = 64$ Gbd - UT

Fig. 6. Correlation coefficient of the 20th span with the preceding $C_{20,j}$, DP-QPSK modulated, with (red) and without (blue) CuT predistortion for $D = 4$ ps/nm/km (squares) and $D = 16$ ps/nm/km (circles). OLS configurations are reported in subcaptions.

ule using SSMF-like fiber, after a NZDSF-2 fiber type. Hence, we may argue that jumping from a low to large dispersion decrases the correlation due to the different characteristic of the noise field itself generated in the two spans. In fact, the second span of SSMF shows back larger correlation with the 9-th span noise. In the UT case the correlation still drops after a couple of spans, however, we may see that in the 2nd module, having lowest dispersion $D = 4$ ps/nm/km, spans are more correlated than the other fiber types as they accumulate less dispersion. Finally, in the mixed fiber - mixed residual case, while the first two DM modules show large and longer correlation memory, the introduction of the 3-rd UT module practically eliminates coherence. Note that this happens at the 10th span, i.e. with one span of *spatial delay*, as it needs the first UT span for the coherence to drop.

In Fig.6 we show the differences among the correlation coeficients obtained in the undistorted and the predistorted case. We show two uniform DM cases ($D_{RES} = 40$ ps/nm and $D_{RES} = 80$ ps/nm) and the UT case, for $D = 4$ ps/nm/km and $D = 16$ ps/nm/km. In each figure we report the correlation coefficient of the 20th span with all the preceding $C_{20,j}$, $(j = 1 \dots 19)$ to get a large picture over the whole OLS. In the DM cases (Fig.6(a),6(b)) we observe that the correlation depends on the dispersion coefficient, although the net dispersion accumulated between the j-th span and 20-th is the same. Also, the C_{ij} estimated applying predistortion always give a worst-case correlation coefficient. However, the most significant contributions come from the very first spans before the 20th, for which the difference between the undistorted/predistorted curves is reduced. In the UT case (Fig.6(c)) we are actually comparing two different residuals, because we get a $D_{RES} = 320$ ps/nm and $D_{RES} = 1280$ ps/nm for $D = 4$ ps/nm/km and $D = 16$ ps/nm/km, respectively. However, in this case the maximum correlation with the 19th span amounts to just 0.25 and gets reduced to 0.1 with larger D.

We have then tested the reconstruction of the overall SCI power per span $\Delta P_{SCI,i}$ using Eq. (10) and compared to the reference simulation outcome. Due to the numerous OLS configurations we report here only some notable cases giving a comprehensive picture of the results. We report the curves for uniform configurations (Tab.1) with the same loss coefficient of $\alpha = 0.2$ dB/km and $R_s = 32$ GBd in Fig.7. First and second rows show two DM case with $D_{RES} = 40$ ps/nm and $D_{RES} = 80$ and the $D = 4$ (left) and $D = 16$ (right). Third row reports the results for the UT case. In each figure, we draw both the undistorted (blue) and predistorted (red) reference curves. The dashed model curves with diamond markers will be understood after the final semi-analytical model presentation in section 6. The predistorted curve is always a worst-case by roughly 3 dB with respect to the undistorted, as expected. Predistorted simulation represents a channel which has already propagated, thus the signal can be considered gaussian distributed and adhering the hypotheses of the GN model, at least at the pure SCI level. In figure we have also reported the ΔP_{SCI} as predicted by the IGN model (black dashed line) and the pure SCI evolution as obtained from the on-off SSFM simulations (dashed-pentagon curves), thus isolating the dispersion effect on the span-intrinsic SCI noise field, i.e. the gaussianization. The gaussianization phenomenon is evident by comparing the pure curves: as the undistorted pure propagation accumulates dispersion it approaches the predistorted pure curve, the latter being constant as it has already enough pre-applied dispersion. In the DM OLS the gaussianization transient is longer becase each span accumulates only 40 or 80 ps/nm per span, while the UT case 320 ps/nm and 1280 ps/nm per span for $D = 4$ ps/nm/km and $D = 16$ ps/nm/km, respectively. The IGN model gives always an accurate estimation of the pure SCI power, conservative by around 1 dB relatively to the predistorted pure curve. The distance between the reference and pure curves is the effect of coherent accumulation. Hence, in the considered DM OLS, the IGN model would underestimate the undistorted SCI at the 20th span by around 9 dB for $D_{RES} = 40$ ps/nm and by 11 dB for $D_{RES} = 80$ ps/nm. UT propagation still shows a smaller coherence: the IGN model underestimates the reference predistorted curve by about 3 dB, however, it stay approximately in the middle of the reference undistorted curve, which still has coherency, but has better QoT due to the ongoing gaussianization process. This explains why the IGN model works so well in UT systems: indeed, due to the low degree of coherence, it trades its conservativeness due to the gaussian hypothesis with the absence of coherence. Finally, we have plotted with circle markers the coherent SCI reconstruction, obtained using the correlation coefficients and the pure curves, for both undistorted and predistorted case. These rebuild the reference curves by combining the pure SCI powers and C_{ij} obtained from the on-off simulations using Eq. (14), to test the validity of the disaggreated approach. The reconstruction approximates well the reference curves in all the cases confirming the validity of the presented approach.

We then report the outcome of the same process on mixed fiber configurations. The results are plotted in Fig.8 for both the symbol rates R_s = 32 GBaud (left column) and R_s = 64 GBaud (right column). We have considered the full UT OLS with DP-

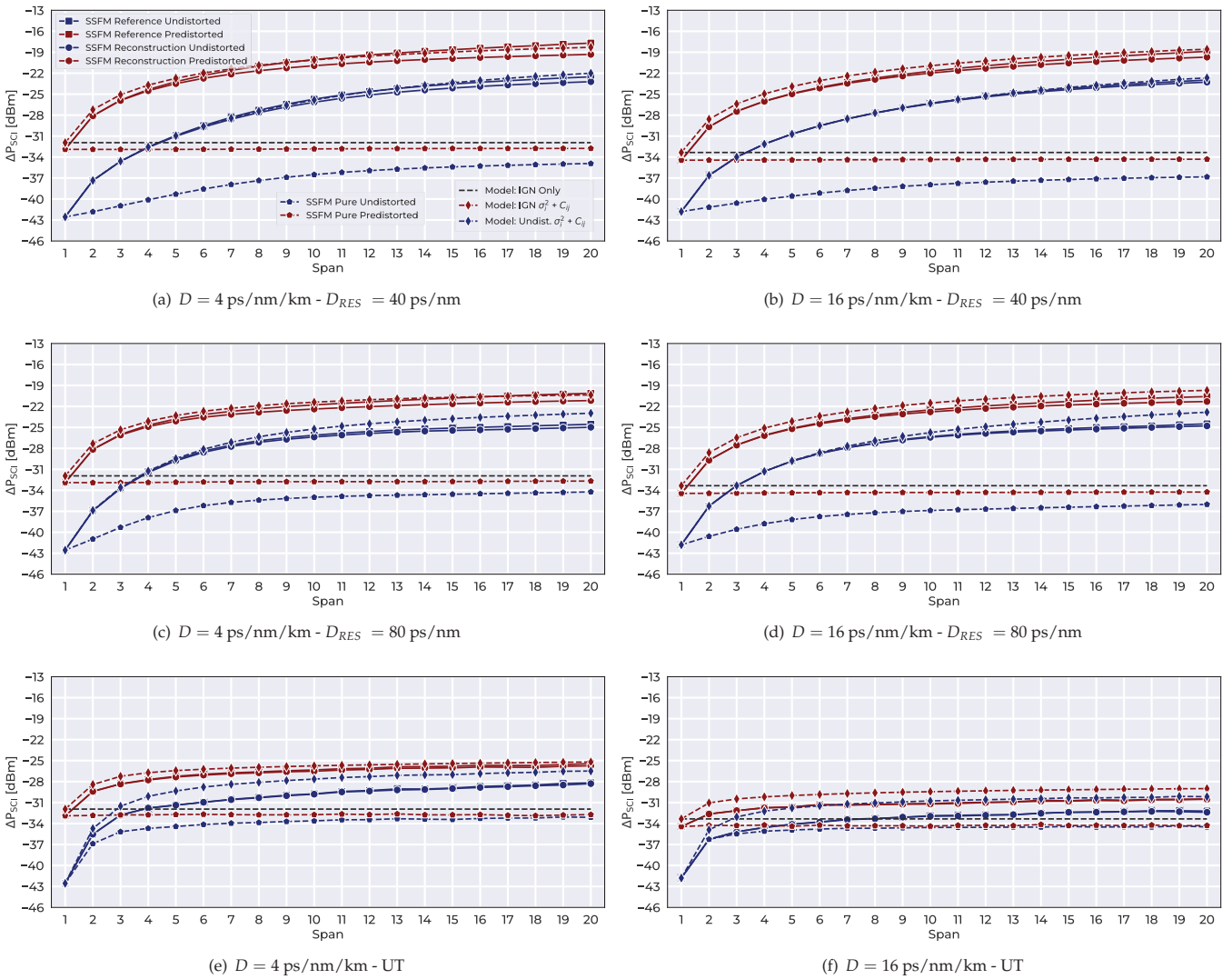

(a) $D = 4$ ps/nm/km - $D_{RES} = 40$ ps/nm

(b) $D = 16$ ps/nm/km - $D_{RES} = 40$ ps/nm

(c) $D = 4$ ps/nm/km - $D_{RES} = 80$ ps/nm

(d) $D = 16$ ps/nm/km - $D_{RES} = 80$ ps/nm

(e) $D = 4$ ps/nm/km - UT

(f) $D = 16$ ps/nm/km - UT

Fig. 7. SCI power per span ΔP_{SCI} for DP-QPSK CuT modulated at $R_s = 32$ Gbd on uniform OLS with: (left column) $D = 4$ ps/nm/km, (right column) $D = 16$ /ps/nm/km. (1st row) $D_{RES} = 40$ ps/nm, (2nd row) $D_{RES} = 80$ ps/nm, (3rd row) UT. Legend in (a) refers to all the figures.

QPSK in the first row and the mixed residual case with DP-QPSK and DP-16QAM in the second and third rows, respectively. With respect to the undistorted and predistorted curves we can observe three different pure SCI intensity levels corresponding to the three different fiber types. The gap between the pure SCI curves is smaller as expected for DP-16QAM, since larger modulation formats tends to the gaussian distribution faster, thanks to the signal levels' larger variability [21, 29]. In the UT case, due to the presence of low dispersion fibers ($D = 4$ ps/nm/km) in the second 4x span module (span 5-8), we observe more coherence in the reference undistorted curve, underestimated by the IGN model, which instead works well in the UT module (span 9-12). Looking at the the mixed residual case instead, we observe large coherence in the first two 4x spans modules with $D_{RES} = 40$ ps/nm and $D_{RES} = 80$ ps/nm. As seen in Fig.5(f), although the first UT span is the 9-th, we see a drop in the additional coherence power at the 10-th span, as the accumulated dispersion seen at the 9-th fiber input is still small due to the previous DM span. At the same point we observe that the reference curve shows actually less SCI than the corresponding pure contributions, which may seem odd as it should include additional coherence power. This may be explained due to a destructive interference between different span contribution, which clearly arise when more than one span has Kerr effect turned on, due to low pulse spreading of the undistorted case. In fact, this effect doesn't show up in the predistorted curve. However, this does not undermine the modelling approach as the pure term is maintained conservative. Also, the usage of a DSP with fixed CPE length may play a role. However, using an adaptive CPE length brings other glitches in the differential SCI measurements which are out of the scope of this paper and do not change the general conclusion of the work. The SCI reconstruction curves are spot on the reference predistorted curves. A very good agreement is shown also on the undistorted case, that we have been able to report only for the DP-16QAM modulated case, although we do not expect different outcomes for DP-QPSK.

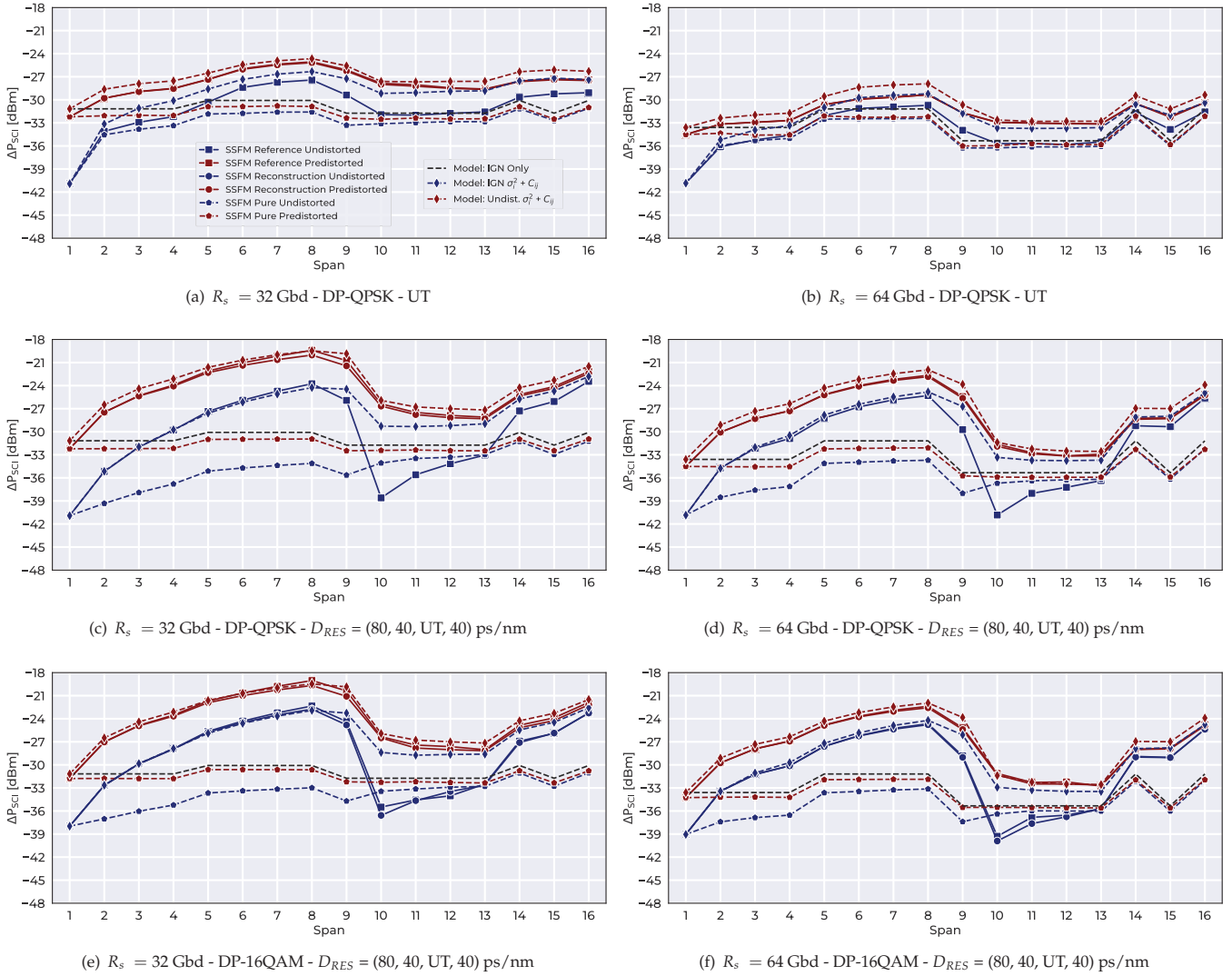

(a) R_s = 32 Gbd - DP-QPSK - UT

(b) R_s = 64 Gbd - DP-QPSK - UT

(c) R_s = 32 Gbd - DP-QPSK - D_{RES} = (80, 40, UT, 40) ps/nm

(d) R_s = 64 Gbd - DP-QPSK - D_{RES} = (80, 40, UT, 40) ps/nm

(e) R_s = 32 Gbd - DP-16QAM - D_{RES} = (80, 40, UT, 40) ps/nm

(f) R_s = 64 Gbd - DP-16QAM - D_{RES} = (80, 40, UT, 40) ps/nm

Fig. 8. SCI power per span ΔP_{SCI} for (1st and 2nd row) DP-QPSK (3rd row) DP-16QAM CuT modulated at (left column) R_s = 32 Gbd (right column) R_s = 64 Gbd on mixed fiber OLS with (1st row) UT, (2nd and 3rd row) D_{RES} = [80, 40, UT, 40] ps/nm. Legend in (a) refers to all the figures.

6. CORRELATION COEFFICIENTS SCALING LAWS

The modeling approach presented in section 4 is based on the statistical correlation of the pure SCI random processes added in each span, allowing to separate the pure and correlation contributions to the total SCI. The simulation results of the previous section have shown that this approach approximates well SCI accumulation. However, for each OLS configuration a large amount of simulations have been run to extract the C_{ij} coefficients, so that understanding the scaling laws of the C_{ij} would be more practical. In particular, by understanding the relationship between the channel characteristic and the spans (i, j) physical parameters with the correlation coefficients, we can develop a semi-analytical model to quickly estimate the coefficients for whatever reasonable system configuration. In [34] we have already observed the scaling of coherent accumulation. However, that was done only on a limited set of uniform UT OLS and we observed only an asymptotic C_∞ aggregating all the span contributions, which scaled down with the product of the squared symbol rate and the accumulated dispersion. Here we prosecute the study of the scaling laws of the correlation coefficient of each couple of span, as the aggregate C_∞ approach cannot be used on a mixed fiber scenario. Thanks to the large set of configurations simulated, we have found out that the C_{ij} coefficients scale almost entirely with the ratio:

$$\frac{\theta^2_{span}(i,j)}{\theta_{eff}(j)} \tag{16}$$

$$\theta_{span}(i,j) = \pi R_s^2 \left| \sum_{k=j}^{i-1} \beta_{2,k} L_{s,k} + \beta_{DCU,k} \right| \tag{17}$$

$$\theta_{eff}(j) = \pi R_s^2 \beta_{2,j} L_{eff,j} \tag{18}$$

The $\theta_{span}(i,j)$ parameter, as in [34], accounts for the accumulated dispersion between the j-th and i-th span input, other than the symbol rate R_s . The scaling by $\theta_{eff}(j)$ corrects for the different correlation observed between two span (i, j) with the same

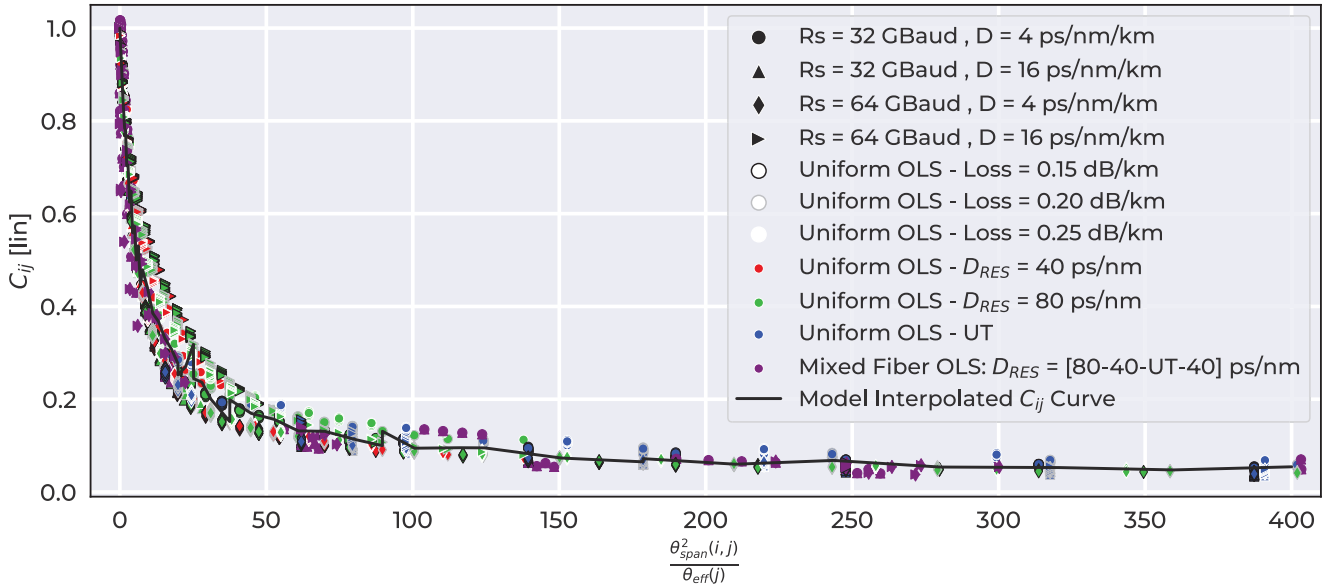

Fig. 9. Correlation coefficients from predistorted on-off simulations vs $\theta^2_{span}(i,j)\,/\theta_{eff}(j)$ parameter. All the combinations of physical parameters of the uniform configurations and the mixed fiber-mixed residuals are reported with different markers (R_s, D combinations), marker edge colors (loss values) and marker face colors (inline residual values). In black, the curve obtained by dataset averaging and interpolation.

$\theta_{span}\,(i,j)$ but different loss coefficient α and dispersion coefficient D. Fig.9 plots on the y-axis the C_{ij} extracted from all the considered uniform simulations set of Tab.1 and the mixed residual case of Tab.2 with respect to their $\theta^2_{span}(i,j)\,/\theta_{eff}(j)$ ratio. We have selected only the C_{ij} obtained from predistorted simulation set because, as in Fig.6, they provide a worst case correlation thus allowing a conservative coherence estimation. Fig.9 shows that the correlation coefficients of all the configurations approximately collapse to a unique curve. This dataset can thus be used to extract an averaged interpolated curve (reported in black in Fig.9) from which, given whatever OLS configuration, we are able to pick the C_{ij} parameter once the characteristic parameter $\theta^2_{span}(i,j)\,/\theta_{eff}(j)$ is known. This allows to calculate the ΔP_{SCI} of a generic system using Eq. (10). To do this however, we still need to estimate the pure SCI terms σ_i . This leads to two versions of the model:

- **Semi-Analytical Undistorted Model**: uses the SSFM simulated undistorted pure SCI terms and adds on top of them the coherency calculated with the worst-case predistorted interpolated C_{ij} curve. As it takes into account the gaussianization transient, it provides more accurate ΔP_{SCI} estimation. However, it relies on the simulated value or in the implementation of computational-hungry models such as the EGN model [29] to estimate the pure SCI terms.
- **Semi-Analytical Predistorted Model**: assumes signal gaussian distribution, thus providing a worst case SCI estimation. The overall SCI evaluation is carried out instantly as the pure SCI terms are estimated using the IGN model.

We have reported the SCI estimated using both semi-analytical model version on Fig.7 for uniform configurations and Fig.8 for mixed fiber configurations. In all the cases, the proposed model follows well the evolution of the SCI introduced at each span. In particular, the predistorted version is very accurate and slightly conservative w.r.t. the reference predistorted curve. Such conservative gap grows to around 3 dB when compared to the undistorted reference curve, which we remark being the characteristic of a newly deployed LP. The undistorted model version improves the prediction with respect to the undistorted reference curve, although the overestimation is larger in the UT sections. We do not notice also any significant change in estimation accuracy with respect to the symbol rate or the modulation format. Hence, this implies a substantial independence of the correlation entity with respect to the modulation format, which instead affects the pure SCI terms gaussianization. In fact, the C_{ij} interpolated curve has been obtained from a dataset where DP-QPSK was the only modulation format considered. This comes quite in handy in the path computation process as it allows to simplify the SCI estimation when the maximum supported modulation format is still to be determined.

A. Non-Transparent OLS

As a last test we have validated the model on an additional $N_s = 5$ spans OLS, whose configuration represents a realistic laboratory setup provided by SM-Optics. Differently from the previous tests, in this case the system is not operated in transparency, i.e. each amplifier does not recover exactly the fiber span loss. This gives us the opportunity to test the model on a mixed fiber system using both SSMF and NZDSF fibers with proper physical parameters and different lengths, residual dispersion and input powers at each span input, thus referring to the most general formula of Eq. (10), but using the same C_{ij} interpolated curve of Fig.9 for coherency estimation. The OLS description of the system is reported in Tab.3. As depicted in Fig.10, each fiber span of the laboratory setup has the DCU connected in between the two stages of the ILAs. The same figure shows the abstraction used for the model estimation of the SCI in this system. The dual stage ILA has been modeled as an ampli-

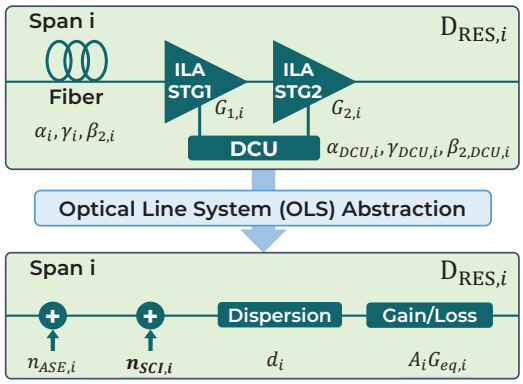

Fig. 10. Block diagram of a span of the non-transparent OLS configuration provided by SM-Optics. At the bottom, its equivalent model with a unique, equivalent ILA.

Table 3. Non-Transparent OLS Configuration

Span	Fiber	L_s $L_{s,DCU}$ km	α α_{DCU} dB/km	D D_{DCU} ps/nm/km	γ γ_{DCU} 1/W/km	P_{ch} $P_{ch,DCU}$ dBm	AG_{eq} dB	D_{RES} ps/nm
1	SSMF	50	0.25	16.7	1.05	3.35	-1.9	5.33
	DCU	7.2	0.43	-118	4.39	-6.16		
2	NZDSF	75	0.25	3.8	1.36	1.45	2.29	-146.6
	DCU	3.8	0.43	-118	4.39	-7.25		
3	SSMF	100	0.25	16.7	1.05	3.74	-1.69	38.3
	DCU	13.9	0.43	-118	4.39	-2.03		
4	NZDSF	25	0.25	3.8	1.36	2.05	2.6	113.4
5	SSMF	125	0.25	16.7	1.05	4.65	-1.3	664.5
	DCU	12.3	0.43	-118	4.39	-1.40		

fier whose equivalent gain is $G_{eq,i} = G_{1,i} - \alpha_{DCU,i} L_{DCU,i} + G_{2,i}$ dB. Tab.3 also reports the gain-loss products of each span $A_g G_{eq,i}$, being A_i the fiber loss $\alpha_i L_{s,i}$ in linear units. The CuT power at each fiber segment input (fiber and DCU) have been reported. We have first ran the entire simulation set for this system (reference and on-off simulations), using both $R_s = 32$ Gbaud and $R_s = 64$ GBaud, undistorted and predistorted, with DP-QPSK and DP-16QAM modulation formats. The channel power launched into the first span, as in the laboratory setup description provided by SM-Optics, is $P_{ch} = 3.35$ dBm. We assume that the SCI generated in the DCU is negligible, as the channel power at the DCU input is usually low to operate in linear regime. In Fig.11 we have simulated the undistorted reference curve with the DCU Kerr effect turned on and off, observing only a small SCI increase (less than 1 dB) w.r.t. the case with DCU Kerr effect off, thus confirming our assumption. We have omitted the pure SCI curves for figure clarity. However, the reference reconstruction for both cases using the simulation set works perfectly. Finally, using the equivalent span model, we have the ran both the semi-analytical model versions and compared their results to the reference simulation. The predistorted model follows tightly the predistorted reference curve evolution, with only a small overestimation. The undistorted version give similarly good results, however, it shows a larger overestimation at the 4th span. As also seen in the undistorted mixed fiber results of Fig.8, this happens when a large decorrelation is introduced due to the insertion of a UT span. We here confirm no significant accuracy difference when going to DP-16QAM at both symbol rates. With respect to the statistical distribution of the signal, we have seen that undistorted and predistorted channels lead to different C_{ij} values. However, the usage of the undistorted semi-analytical model (based on predistorted C_{ij} curve) only leads to a relatively small SCI overestimation, so that, for practical purposes, we may think to approach the coherency estimation and gaussianization problems separately: the former affecting the interaction between pure SCI terms, the latter affecting the intensity of the pure SCI terms alone.

7. SCI COHERENCY WEIGHT ON OVERALL QOT

We have shown that neglecting coherent accumulation in DM OLSs may lead to underestimate the SCI contribution to NLI by several dB. We now assess how much such SCI underestimation impacts the overall GSNR evaluation considering also to fill the spectrum with other interfering channels. To this aim we have considered two mixed fiber OLSs as in Tab.2. In the first case, we consider the mixed residual configuration, so that span 1-4 have $D_{RES} = 80$ ps/nm, span 5-8 and 13-16 $D_{RES} = 40$ ps/nm, span 9-12 are UT. We considered for this OLS two spectral loads with $N_{ch} = 5$ and 15 400G channels ($R_s = 64$ Gbaud, DP-16QAM, 75 GHz WDM grid, accordingly to OpenZR+ [1] MSA) launched at $P_{ch} = 1$ dBm. In the $N_{ch} = 5$ load (Tab.4 Case #1) the 3rd channel is the CuT and they are all spaced by 150 GHz to simulate a sparse channel allocation. In the $N_{ch} = 15$ load (Tab.4 Case #2), instead, the 7th channel is the CuT and they are all spaced by the 75 GHz standard. Both scenarios have limited channel allocation because when coherent channels are deployed on DM OLSs, part of the spectrum may be already filled with legacy IMDD 10G channels and a guard-band between the two technologies must be maintained to avoid out of service [28]. The QoT degradation due to possible copropagating 10G IMDD channels has been neglected, although it maybe considered using the model in [28]. For the second OLS we consider the same mixed fiber types OLS of Tab.2 but all spans are kept UT. In this case we fill the spectrum with $N_{ch} = 64$ 400G channels at $P_{ch} = 1$ dBm on the entire C-band, being the center 33-th channel the CuT (Tab.4 Case #3). The three considered configurations are summarized in Tab.4, with all channels always launched in the system without any predistortion.

First we have simulated both scenarios and obtain the evolution of the total NLI $\Delta P_{NLI,i}$, thus including both SCI and XCI noise. These reference simulations are reported in yellow, continuous curves in the NLI components figures of Fig.12(a,c,e). The coherent SCI component $\Delta P_{SCI,i}$ (blue in Fig.12(a,c,e)) has been obtained with single channel simulations. Then, the ΔP_{XCI} component due to all the interfering channels (reported in red in

Table 4. GSNR Weight System Configuration

R_s = 64 GBaud - DP-16QAM

4x Modules of 4x Spans with Mixed Fiber Types (Tab.2)

Use Case	400G N_{ch}	D_{RES} per Span Module
Case #1	5	80 - 40 - UT - 40
Case #2	15	80 - 40 - UT - 40
Case #3	64	UT - UT - UT - UT

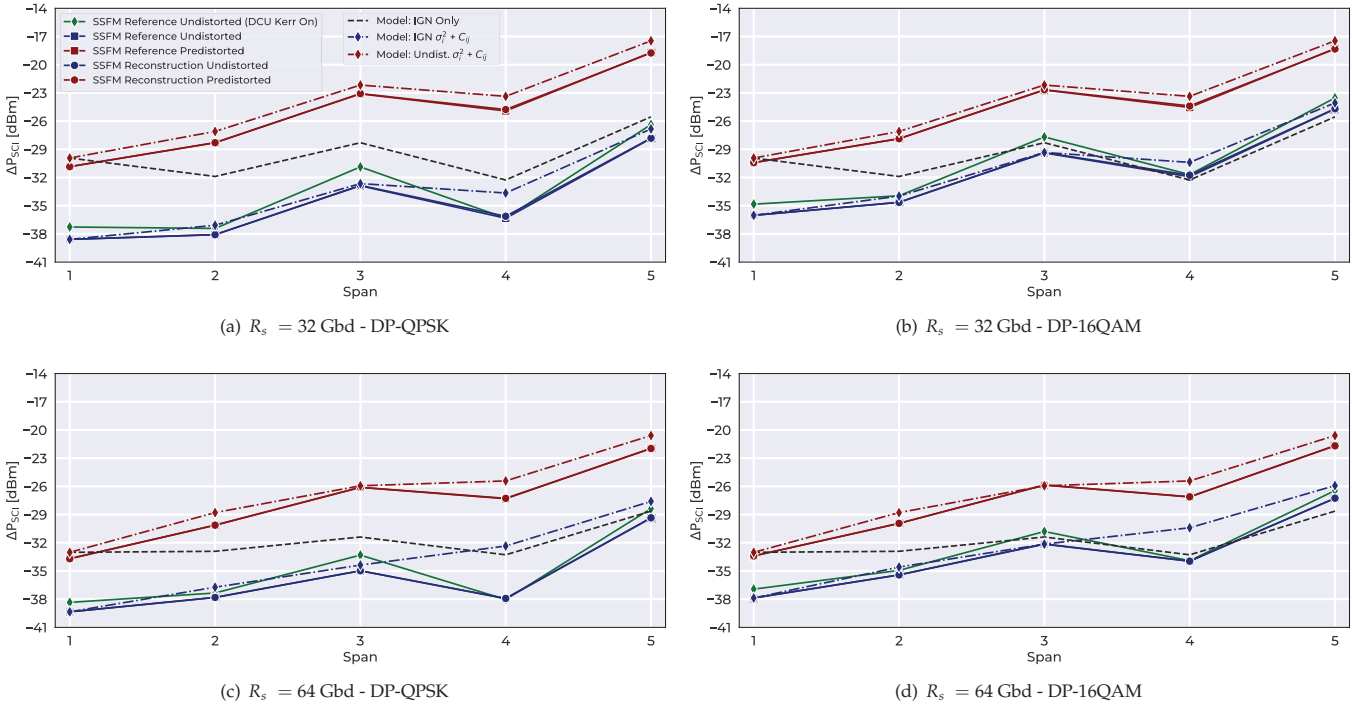

(a) R_s = 32 Gbd - DP-QPSK

(b) R_s = 32 Gbd - DP-16QAM

(c) R_s = 64 Gbd - DP-QPSK

(d) R_s = 64 Gbd - DP-16QAM

Fig. 11. SCI power per span ΔP_{SCI} for (left column) DP-QPSK (right column) DP-16QAM CuT modulated at (1st row) R_s = 32 Gbd (2nd row) R_s = 64 Gbd on a non-transparent OLS. Legend in (a) refers to all the figures.

Fig.12(a,c,e)) has been obtained by simulation of the whole DWDM comb but keeping the CuT power low to exclude SCI. The same figures also reports the superposition of the simulated XCI and SCI obtained as from Eq. (2) (yellow dashed curve) which is in accordance with the reference one. In case #1 the SCI is predominant on the XCI due to the low number of interfering channels and stronger coherence, but becomes almost equal when going to 15 channel load (case #2). In the UT systems instead the XCI is always predominant due to the larger number of channel and the less intense SCI coherent accumulation. Fig.12(a,c,e) also reports the overall NLI estimation using the IGN model for SCI (grey) and the two coherent model versions of Eq. (10) for SCI (green and purple). These curves are obtained by adding the simulated XCI to the estimated SCI, as the XCI in DM OLS is out of the scope of this work. We may notice that the model outcomes using IGN is never conservative w.r.t. the real performance of the reference curve (yellow), although the gap is very small in the UT OLS. However, we should remark that in UT system this happens because the XCI is obtained by simulation, so it lacks of the additional overestimation that the IGN model for XCI would add. In the DM cases (cases #1, #2), the usage of IGN only for the SCI component underestimates the whole NLI up to more than 3 dB. Both the predistorted (purple) and undistorted (green) semi-analytical models for SCI instead follow well the evolution of the overall NLI in both the DM and UT mixed fiber OLS and always gives a conservative estimation, although their difference is very small, also w.r.t. the IGN model curve in the UT system.

Finally, we estimate the accumulated GSNR at end of each span using the different models solutions. To do this we assume that the ILAs are operated in transparency and they have a noise figure of 6.2 dB, which is common in terrestrial networks scenario. From this hypothesis we calculate the amount of ASE noise added in each span. By cumulative summing the NLI and ASE noise contribution introduced at each span we obtain the accumulated SNR_{NLI} and $OSNR$. Then, the GSNR is obtained using Eq. (1). The GSNR curves are plotted in Fig.12(b,d,f) using the three considered SCI modeling approaches for the three considered spectral loads/OLSs. We also report the GSNR threshold (in R_s bandwidth) for 400G (16.9 dB) of the OpenZR+ standard [1] to discuss the implications of the SCI underestimation in path feasibility. As we see from the reference (yellow) curve, all the configurations can cover transmission up to 6 spans, although there is no margin for case #2 (DM) with N_{ch} = 15 so we may consider its reach of 5 spans. In the UT case #3, the IGN model approach works well in predicting the actual reach as the SCI coherency is small. The coherency models presented in this paper instead are slightly more conservative than IGN but still correctly predicts the actual reach of the system. In the DM setups (cases #1, #2), instead, the IGN approach overestimates the GSNR by about 1 dB (case #1) and 0.5 dB (case #2), which would have led to a wrong estimation of the reach up to 7 spans in the former with N_{ch} = 5 and would not ensure any margin for N_{ch} = 15 thus leading to a possible out of service, which is instead prevented by the undistorted semi-analytical model. The predistorted semi-analytical model instead is more conservative conservative w.r.t. the reference (as it has been simulated without any predistortion, i.e. as it was a newly deployed LP), but still ensuring to operate always on the safe side. In this situation instead the undistorted analytical model correctly predicts the available GSNR with a negligible gap to the reference simulation.

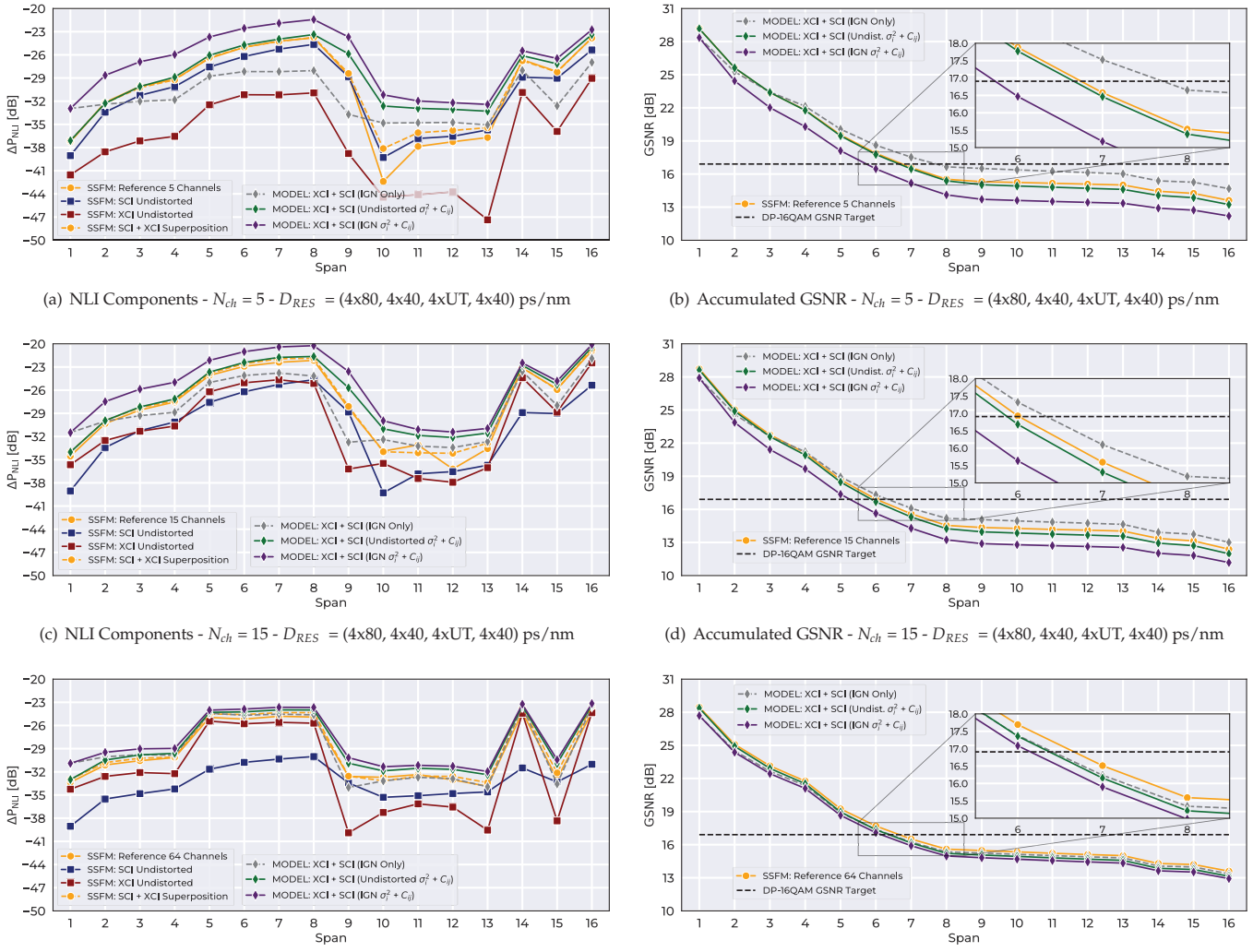

(a) NLI Components - N_{ch} = 5 - D_{RES} = (4x80, 4x40, 4xUT, 4x40) ps/nm

(b) Accumulated GSNR - N_{ch} = 5 - D_{RES} = (4x80, 4x40, 4xUT, 4x40) ps/nm

(c) NLI Components - N_{ch} = 15 - D_{RES} = (4x80, 4x40, 4xUT, 4x40) ps/nm

(d) Accumulated GSNR - N_{ch} = 15 - D_{RES} = (4x80, 4x40, 4xUT, 4x40) ps/nm

(e) NLI Components - N_{ch} = 64 - D_{RES} = UT

(f) Accumulated GSNR - N_{ch} = 64 - D_{RES} = UT

Fig. 12. NLI components per span (right column) and Accumulated GSNR (right column) with model estimations on a mixed fiber OLS: N_{ch} = 5 (1st row) channels and N_{ch} = 15 (2nd row) with D_{RES} = [4x 80, 4x 40, 4x UT, 4x 40] ps/nm. N_{ch} = 64 channels with UT spans (3rd row).

8. CONCLUSIONS

In this work we have analyzed the coherent accumulation of SCI noise induced by Kerr effect on the propagation of a single coherent optics channel on a generic OLS with and without dispersion compensation. We have carried an extensive set of SSFM simulations to observe the scaling of SCI coherent accumulation with different symbol rate and modulation formats as available in commonly deployed flexible rate transceiver. We have observed a strong coherent accumulation of SCI in DM systems, mainly due to the low rate of chromatic dispersion accumulation. To improve the network flexibility and fully exploiting the deployed fiber infrastructure, we have proposed a semi-analytical model to enable QoT estimation of coherent channels routed through segments of DM systems, as traditional models are not able to provide an adequately conservative SCI estimation in this scenario. The developed model has been thought to be employed in online network control, thus being able to provide quick and conservative SCI estimations in realistic OLS made up of mixed fiber types and both DM and UT transmission. Two versions of the model have been proposed: one is based on the quick estimation of the span's pure SCI noise using IGN model and adding the coherency additional power on top of that, but delivering a worst-case estimation for a newly deployed LP since it assumes signal gaussianity due to previous propagation. The second version takes into account non-gaussian signal distribution but requires the intrinsic span SCI noise to be estimated by means of more computationally complex tools. In both cases, we have shown that properly considering coherent SCI accumulation enables correct GSNR calculation in DM OLS, provided that XCI is adequately modeled and avoids overestimation of LP reach. Future investigations will be focused on improving the estimation accuracy and computational burden of the non predistorted model version with simplified (semi)-analytical tools accounting for signal non-gaussianity.

REFERENCES

1. "Openzr+ msa," http://https://openzrplus.org/.
2. A. A. M. Saleh and J. M. Simmons, "All-optical networking—evolution, benefits, challenges, and future vision," Proc. IEEE **100**, 1105–1117 (2012).
3. E. L. Rouzic, O. Augizeau, O. Renais, J. Meuric, T. Marcot, C. Betoule, G. Thouenon, A. Triki, M. Laye, N. Pelloquin, Y. Lagadec, and E. Delfour, "Automation journey in core and metro networks: an operator view," in *2021 European Conference on Optical Communication (ECOC),* (2021), pp. 1–4.
4. G. Borraccini, A. D'Amico, S. Straullu, A. Nespola, S. Piciaccia, A. Tanzi, G. Galimberti, S. Bottacchi, S. Swail, and V. Curri, "Cognitive and autonomous qot-driven optical line controller," J. Opt. Commun. Netw. **13**, E23–E31 (2021).
5. V. Curri, "Software-defined wdm optical transport in disaggregated open optical networks," in *2020 22nd International Conference on Transparent Optical Networks (ICTON),* (2020), pp. 1–4.
6. J. Kundrát, O. Havliš, J. Jedlinský, and J. Vojtěch, "Opening up roadms: Let us build a disaggregated open optical line system," J. Light. Technol. **37**, 4041–4051 (2019).
7. M. Birk, O. Renais, G. Lambert, C. Betoule, G. Thouenon, A. Triki, D. Bhardwaj, S. Vachhani, N. Padi, and S. Tse, "The openroadm initiative [invited]," J. Opt. Commun. Netw. **12**, C58–C67 (2020).
8. C. Manso, R. M. noz, N. Yoshikane, R. Casellas, R. Vilalta, R. Martínez, T. Tsuritani, and I. Morita, "Tapi-enabled sdn control for partially disaggregated multi-domain (ols) and multi-layer (wdm over sdm) optical networks," J. Opt. Commun. Netw. **13**, A21–A33 (2021).
9. R. Casellas, R. Martínez, R. Vilalta, and R. Muñoz, "Abstraction and control of multi-domain disaggregated optical networks with openroadm device models," J. Light. Technol. **38**, 2606–2615 (2020).
10. F. Cugini, F. Paolucci, F. Fresi, G. Meloni, N. Sambo, L. Potí, A. D'Errico, and P. Castoldi, "Toward plug-and-play software-defined elastic optical networks," J. Light. Technol. **34**, 1494–1500 (2016).
11. S. Abdelwahab, B. Hamdaoui, M. Guizani, and T. Znati, "Network function virtualization in 5g," IEEE Commun. Mag. **54**, 84–91 (2016).
12. M. Filer, H. Chaouch, and X. Wu, "Toward transport ecosystem interoperability enabled by vendor-diverse coherent optical sources over an open line system," J. Opt. Commun. Netw. **10**, A216–A224 (2018).
13. P. Poggiolini, "The gn model of non-linear propagation in uncompensated coherent optical systems," J. Light. Technol. **30**, 3857–3879 (2012).
14. A. Carena, V. Curri, G. Bosco, P. Poggiolini, and F. Forghieri, "Modeling of the impact of nonlinear propagation effects in uncompensated optical coherent transmission links," J. Light. Tech. **30**, 1524–1539 (2012).
15. A. Mecozzi and R.-J. Essiambre, "Nonlinear shannon limit in pseudo-linear coherent systems," J. Light. Technol. **30**, 2011–2024 (2012).
16. E. London, E. Virgillito, A. D'Amico, A. Napoli, and V. Curri, "Simulative assessment of non-linear interference generation within disaggregated optical line systems," OSA Continuum **3**, 3378–3389 (2020).
17. P. Poggiolini, G. Bosco, A. Carena, V. Curri, Y. Jiang, and F. Forghieri, "A detailed analytical derivation of the gn model of non-linear interference in coherent optical transmission systems," (2014).
18. P. Johannisson and M. Karlsson, "Perturbation analysis of nonlinear propagation in a strongly dispersive optical communication system," J. Light. Tech. **31**, 1273–1282 (2013).
19. A. Bononi, O. Beucher, and P. Serena, "Single- and cross-channel nonlinear interference in the gaussian noise model with rectangular spectra," Opt. Express **21**, 32254–32268 (2013).
20. P. Serena and A. Bononi, "An alternative approach to the gaussian noise model and its system implications," J. Light. Technol. **31**, 3489–3499 (2013).
21. R. Dar, M. Feder, A. Mecozzi, and M. Shtaif, "Pulse collision picture of inter-channel nonlinear interference in fiber-optic communications," J. Light. Technol. **34**, 593–607 (2016).
22. P. Serena and A. Bononi, "A time-domain extended gaussian noise model," J. Light. Technol. **33**, 1459–1472 (2015).
23. E. London, A. D'Amico, E. Virgillito, A. Napoli, and V. Curri, "Modelling non-linear interference in non-periodic and disaggregated optical network segments," Opt. Continuum **1**, 793–803 (2022).
24. "Github repository of gnpy," https://doi.org/10.5281/zenodo.3458319.
25. V. Curri, "Gnpy model of the physical layer for open and disaggregated optical networking," J. Opt. Commun. Netw. **14**, C92–C104 (2022).
26. A. D'Amico, E. London, B. L. Guyader, F. Frank, E. L. Rouzic, E. Pincemin, N. Brochier, and V. Curri, "Experimental validation of gnpy in a multi-vendor flex-grid flex-rate wdm optical transport scenario," J. Opt. Commun. Netw. **14**, 79–88 (2022).
27. E. Virgillito, R.-P. Braun, D. Breuer, A. Gladisch, V. Curri, and G. Grammel, "Testing tip open source solutions in deployed optical networks," in *Optical Fiber Communication Conference (OFC) 2021,* (Optical Society of America, 2021), p. F1C.3.
28. E. Virgillito, A. Castoldi, S. Straullu, R. Pastorelli, and V. Curri, "Qot computation for 100g lightpaths routed on 10g-loaded dispersion-managed network segments," in *2021 International Conference on Electrical, Communication, and Computer Engineering (ICECCE),* (2021), pp. 1–6.
29. A. Carena, G. Bosco, V. Curri, Y. Jiang, P. Poggiolini, and F. Forghieri, "Egn model of non-linear fiber propagation," Opt. express **22**, 16335–16362 (2014).
30. P. Poggiolini, G. Bosco, A. Carena, V. Curri, Y. Jiang, and F. Forghieri, "A simple and effective closed-form gn model correction formula accounting for signal non-gaussian distribution," J. Light. Technol. **33**, 459–473 (2015).
31. E. Virgillito, A. Castoldi, A. D'Amico, S. Straullu, R. Bratovich, F. M. Rodriguez, A. Bovio, R. Pastorelli, and V. Curri, "Spatially Disaggregated Modelling of Self-Channel NLI in Mixed Fibers Optical Transmission," in *European Conference on Optical Communication (ECOC) 2022 (2022), Paper Tu5.32,* (Optica Publishing Group, 2022), p. Tu5.32.
32. A. D'Amico, E. London, E. Virgillito, A. Napoli, and V. Curri, "Quality of transmission estimation for network planning: how to handle single-channel nonlinear effects?" (2019).
33. A. Mecozzi, C. Clausen, and M. Shtaif, "Analysis of intrachannel nonlinear effects in highly dispersed optical pulse transmission," IEEE Photonics Technol. Lett. **12**, 392–394 (2000).
34. A. D'Amico, E. London, E. Virgillito, A. Napoli, and V. Curri, "Quality of transmission estimation for planning of disaggregated optical networks," in *2020 International Conference on Optical Network Design and Modeling (ONDM),* (2020), pp. 1–3.
35. P. Poggiolini and Y. Jiang, "Recent advances in the modeling of the impact of nonlinear fiber propagation effects on uncompensated coherent transmission systems," J. Light. Technol. **35**, 458–480 (2017).